Structural Mechanism for Heparin-Binding of the Third Kunitz Domain of Human Tissue Factor Pathway Inhibitor[†,‡]

Shouhei Mine,[||] Toshio Yamazaki,[§] Toshiyuki Miyata,[||] Saburo Hara,[⊥] and Hisao Kato*[,||]

National Cardiovascular Center Research Institute, 5 Fujishirodai, Suita, Osaka 565-8565 Japan, Institute for Protein Research, Osaka University, 3-2 Yamadaoka, Suita, Osaka 565-0871, Japan, and Kyoto Institute of Technology, Matsugasaki, Sakyo-ku, Kyoto 606-8585, Japan

Received June 20, 2001; Revised Manuscript Received October 19, 2001

ABSTRACT: Tissue factor pathway inhibitor (TFPI) inhibits the activity of coagulation factor VIIa and Xa through its K1 and K2 domain, respectively, and the inhibitory activity is enhanced by heparin. The function of the K3 domain of TFPI has not been established, but the domain probably harbors a heparin binding site (HBS-2). We determined the three-dimensional solution structure of the TFPI K3 domain (Glu182−Gly242) by heteronuclear multidimensional NMR. The results showed that the molecule is composed of one antiparallel β-sheet and one α-helix, and in overall structure is very similar to the K2 domain, with the rms deviation of 1.55 Å for the 58 defined C^{α} positions. However, the surface electrostatic properties of both domains are different each other. The lack of inhibitory activity of the K3 domain is explained by the absence of electrostatic interaction with factor Xa over a large surface area. A titration experiment with size-fractionated heparin showed that a heparin binding site was located in the vicinity of the α-helix. In this region, a positively charged cluster is formed by Lys213, Lys232, and Lys240, and the negatively charged sulfate groups of heparin bind there. The enhancement of inhibitory activity by heparin probably was not due to a conformational change to TFPI itself. It is likely that heparin simply increases the local concentration of TFPI on the cell surface and stabilizes the initial complex that forms.

The exposure of tissue factor (TF)[1] upon vascular injury to the endothelium initiates the extrinsic pathway of coagulation, which involves the sequential activation of a number of plasma serine proteases through limited proteolysis (*1*). This cascade is initiated by the association of TF with coagulation factor VII, the latter being converted to activated factor VII (VIIa). The TF/VIIa complex then activates both factors IX and X, leading to thrombin generation and fibrin-clot formation. Therefore, the initiation of the TF pathway must be under basal level inhibition to maintain hemostasis.

Tissue factor pathway inhibitor (TFPI) is a 36-kDa protease inhibitor that consists of three tandem Kunitz-type domains and a basic C-terminal region (Figure 1). TFPI circulates in the blood stream in association with lipoproteins such as VLDL/LDL and HDL as well as in a free form (*2*). TFPI is also located in blood platelets (*3*), but the majority of TFPI is supposed to be associated with proteoglycan on the surface of endothelial cells and is released by heparin (*4*−*6*). TFPI blocks the TF-initiated coagulation pathway by inhibiting both factor Xa and the factor VIIa/TF complex (*7*), thereby inhibiting TF activity. The inhibition of factor Xa is caused by the TFPI Kunitz 2 (K2) domain and that of the VIIa/TF complex by the TFPI Kunitz 1 (K1) (*8*) domain. However, the TFPI Kunitz 3 (K3) domain does not bind to either enzyme by itself, and its function has not been firmly established. The sequence identity of the K3 domain with the K1 and the K2 domain is around 43%, respectively (Figure 1). The structure of the TFPI K2 domain in complex with trypsin has already been determined by X-ray crystallography, and the mechanism of the interaction between the K2 domain and factor Xa has been discussed (*9*). In addition, the structure of VIIa/TF with BPTI mutant (a homologue of the TFPI K1 domain) has been investigated to elucidate the function of the K1 domain (*10*). But the structure of the K3 domain has not been determined.

The inhibitory activity of TFPI is enhanced in the presence of heparin (*11*−*13*). One of the heparin-binding sites has been postulated to lie in the C-terminal tail (HBS-1), which contains repeated Lys and Arg residues (Figure 1) (*6*). However, TFPI that lacks the C-terminal portion (TFPI-ΔC) could still bind heparin, suggesting the presence of a second heparin binding site (HBS-2) (*14*). Furthermore, it has been reported that a synthetic peptide (Gly212−Phe242) that is a part of the TFPI K3 domain had strong affinity to heparin and the inhibitory activity of TFPI-ΔC was markedly enhanced by heparin (*15*). These results indicate that

[†] This work was supported by the Program for Promotion of Fundamental Studies in Health Sciences of the Organization for Pharmaceutical Safety and Research of Japan.

[‡] The coordinates for 20 NMR structures of the TFPI K3 domain have been deposited in the Protein Data Bank, accession number 1IRH.

* Correpondence should be addressed to this author. Tel: 81-6-6833-5012. Fax: 81-6-6872-8091. E-mail: hkato@ri.ncvc.go.jp.

[||] National Cardiovascular Center Research Institute.

[§] Osaka University.

[⊥] Kyoto Institute of Technology.

[1] Abbreviations: TFPI, tissue factor pathway inhibitor; K1 domain, first Kunitz domain; K2, second Kunitz domain; K3, third Kunitz domain; HSQC, heteronuclear single quantum coherence; TF, tissue factor; VIIa, activated factor VII; TFPI-ΔC, TFPI that lacks the C-terminal portion; HBS-1, first heparin binding site; HBS-2, second heparin binding site.

10.1021/bi011299g CCC: $22.00
Published on Web 12/08/2001

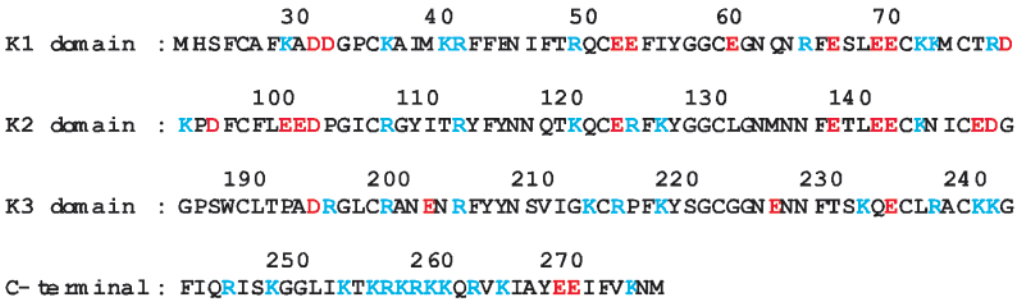

FIGURE 1: Alignment of the amino acid sequence of the human TFPI Kunitz domain. Basic and acidic residues are shown in blue and red, respectively.

functional HSB-2 is located in the TFPI K3 domain between Gly212 and Phe243.

It has been well accepted that there is a close relationship between the structure and function of a protein. Therefore, in the present study, we determined the three-dimensional solution structure of the TFPI K3 domain (Glu182−Gly242) by multidimensional NMR to identify HBS-2 and elucidate the mechanism of the interaction of TFPI with heparin. Furthermore, we compared the structures of the K2 and K3 domains to explain the functional differences between them. We here discuss the heparin-binding ability and the lack of inhibitory activity of the K3 domain from a structural point of view.

MATERIALS AND METHODS

Protein Preparation. An expression vector containing the recombinant human TFPI K3 domain was constructed in the methylotrophic yeast *Pichia pastoris*. Human TFPI K3 domain cDNA was amplified by PCR with the following oligonucleotide primers: 5′-CCCGCCTCGAGAAAAGA-GAATTTCACGGTCCCTCATG-3′ (*Xho*I) and 5′-GCGGG-GAATTCTCAACCTTTTTTACATGCCCTC-3′ (*Eco*RI).

The PCR product was digested with *Xho*I and *Eco*RI and inserted between the *Xho*I and *Eco*RI sites of the *P. pastoris* expression vector pPCI9 (Invitrogen). *P. pastoris* GS115 was transformed with linear-fragmented pPIC9 by digestion with *Sal*I. The DNA sequence of the insert was confirmed using a BigDye Terminator Cycles Sequencing FS Ready Reaction kit (PerkinElmer Life Science).

The fermentation of *P. pastoris* was performed with Basal Salts medium plus PTM1 salts, as described in the Instruction Manual for Pichia Expression kit (Invitrogen). The culture supernatant was harvested by centrifugation 100 h after the start of methanol induction and diluted in a 10-fold volume of buffer containing 50 mM CH_3COONa (pH 4.5), 50 mM NaCl, and 1 mM EDTA. Then, the supernatant was applied onto CM Sepharose FF (Amersham Pharmacia Biotech), and the bound proteins were eluted with a linear gradient of 0.05 to 0.8 M NaCl in 50 mM CH_3COONa (pH 4.5) and 1 mM EDTA. The peak was collected and was purified by reversed-phase HPLC using a C8 μ-Bondasphere column (150 × 3.9 mm: Waters) with an acetonitrile gradient in 0.1% acetic acid. The N-terminal sequence of the purified protein was confirmed using a protein sequencer model 473A (Applied Biosystems). For preparation of uniformly ^{15}N- and ^{13}C-labeled protein, ^{15}N ammonium liquid, $^{13}C^3$-glycerol, and ^{13}C-methanol (Shoko Co., Ltd) were used.

Heparin-Derived Oligosaccharides. Bovine intestinal heparin is a product of Viobin Corp. (Waunakee, WI). Prior to selective deaminative cleavage of glucosamine residues carrying free amino groups with nitirous acid (*16*), heparin was partially *N*-desulfated as described by Nagasawa and Inoue (*17*). Briefly, 1.0 g of heparin was dissolved in 50 mL of water and passed through an Amberlite IR-120 column (Rohm and Hass, H^+ form, 2.5 × 10 cm) at 4 °C. The effluent and the washing were combined and immediately neutralized to pH 7.0 with pyridine and lyophilized. The resulting prydinium salt of heparin (0.99 g) was dissolved in 50 mL of dimethylsulfoxide containing 5% water and allowed to stand for 20 min at 20 °C. After being diluted with an equal volume of water, the solution was neutralized to pH 9.0 with 0.1 N sodium hydroxide, dialyzed against distilled water for 2 days, and lyophilized. The resulting partially *N*-desulfated heparin (0.98 g) was dissolved in water (10 mL), mixed with 200 mL of 0.2 M citrate acid, and adjusted to pH 4.0 with 1 N sodium hydroxide. Then, 10 mL of 2 M sodium nitrite was added, and the solution was allowed to stand for 60 min at 20 °C. After decomposition of the excess nitrite with 20 mL of 7% ammonium sulfamate for 60 min at 20 °C, the solution was concentrated to 15 mL in vacuo to obtain a mixture of heparin-derived oligosaccharides with various chain lengths. The oligosaccharide mixture containing inorganic salts used in the degradation process was then directly subjected to gel filtration using serially connected columns of Biogel P-6 and Biogel P-10 (Bio-Rad, 4.0 × 100 cm each) equilibrated with 0.5 M ammonium bicarbonate, and the sample was eluted with the same solution. The effluent was subjected to a carbazole test (*18*) for detection of uronic acid containing heparin-derived oligosaccharides. The oligosaccharides ranging from disaccharides to eicosaccharides (2mer to 20mer) were further purified by rechromatography under identical conditions and desalted with a Biogel P-2 column (Bio-Rad, 2.5 × 60 cm) using water as eluant, with which the sulfate-containing oligosaccharide is eluted at the void volume of the column.

NMR Measurement. The NMR spectra were collected at 25 °C on Bruker 600 and 800 MHz (Bruker DRX600 and DRX800) instruments equipped with triple-axis-gradient and triple-resonance probes. NMR samples were prepared at 1 mM concentration in 10 mM potassium phosphate buffer (pH 6.0) in 90% H_2O/10% D_2O (v/v). All spectra were processed with nmrPipe and analyzed with nmrDraw and PIPP (*19*, *20*).

Sequential assignments of backbone resonances for recombinant TFPI K3 were achieved using HNCACB and CBCA(CO)NH spectra (*21*, *22*). Aliphatic and aromatic side-chain assignments were obtained from 3D HCCH-TOCSY

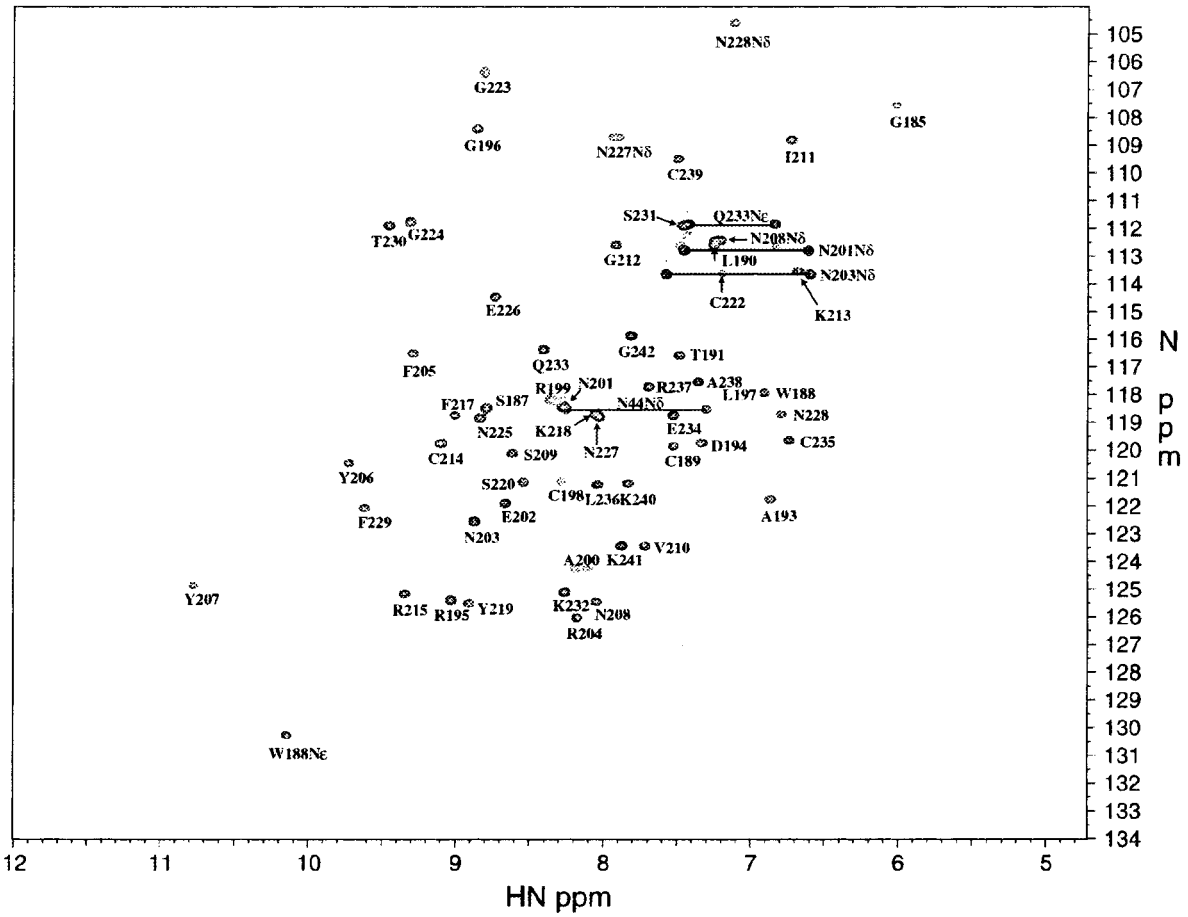

FIGURE 2: ^{1}H-^{15}N HSQC spectrum of the TFPI K3 domain at 25 °C and pH 6. Assignments of backbone signals are indicated by single-letter code and residue number.

and 3D ^{13}C-edited NOESY-HSQC spectra (*23*, *24*). Side-chain amide protons of asparagines and glutamines were assigned on the basis of NOEs to β and γ protons.

The majority of distance restrains were obtained from 3D ^{15}N-edited NOESY-HSQC (*25*) and 3D ^{13}C-edited NOESY-HSQC spectra with a mixing time of 200 ms. The NOE connectivities from strong, medium and cross-peaks were categorized and assumed to correspond to the upper limits for proton−proton distances of 3.0, 4.0, and 5.0 Å, respectively. Methyl, methylene, and aromatic ring protons that were not stereospecifically assigned were treated as pseudo atoms. The ϕ angle restraints were obtained from $^{3}J_{HN,H\alpha}$ coupling constants measured in HMQC-J experiments (*26*). $^{3}J_{HN,H\alpha}$ values of less than 5 Hz, more than 8 Hz, and above 10 Hz were converted to dihedral angle restraints of $-90° \leq \phi \leq -30°$, $-160° \leq \phi \leq 80°$, and $-140° \leq \phi \leq 100°$, respectively. Hydrogen bonds were determined by scalar coupling $^{3h}J_{HN,CO}$ measured in HNCO-TROSY experiments. Hydrogen bonding restraints (two per hydrogen bond) were incorporated as $r_{HN-O} = 1.8-2.2$ Å and $r_{N-O} = 2.2-3.3$ Å.

Structural Calculations. Structural calculations were performed on a Silicon Graphics OCTANE using the simulated annealing protocol with X-PLOR version 3.1 (*27*). Forty structures were generated. Each structure was subjected to 12000 steps of high-temperature dynamics at 2000 K for total of 60 ps, and then cooled to 100 K over a period of 30 ps (6000 steps at 5 fs/step), followed by 200 steps of restrained energy minimization. The force constants of the distance restraints and dihedral angle restraints were 50 kcal mol^{-1} Å^{-2} and 200 kcal mol^{-1} rad^{-2}, respectively. The final family of 20 structures was chosen based on low XPLOR energies, agreement with experimental constraints, and the quality of the structures as determined using the programs PROCHECK (*28*). The coordinates and input constraints have been deposited in the Protein Data Bank (accession code 1IRH for the ensemble of 20 structures).

RESULTS

NMR Assignments and Structure Determination of the TFPI K3 Domain. For multinuclear NMR experiments, the recombinant human TFPI K3 (Glu182−Gly242) domain was labeled with either ^{13}C/^{15}N or only ^{15}N. The assignments of the backbone NH were carried out using 3D HNCACB and HNCO. The side-chain resonance assignments were also obtained by using 3D HCCH-TOCSY on the basis of the main-chain assignments. Figure 2 shows the backbone ^{1}H and ^{15}N assignments on the ^{1}H-^{15}N HSQC spectrum for 54 of the 58 expected peaks (total of 61 residues minus 3 Pro). The four missing backbone HN resonances are N-terminal residues (Glu182, Phe183, and His184) and Gly221. Among the residues visible on the ^{1}H-^{15}N HSQC spectrum, the intensities of Leu197, Cys198, Arg199, Ala200, and Cys222 were markedly low. In addition, the side-chain resonances of these residues except Cys222 could not be observed, suggesting conformational exchange of these residues. This is probably a result of the isomerization of the disulfide bond of Cys198−Cys222, which causes a broadening of the NMR signals in the vicinity of these cysteine residues. Such an

Table 1: Experimental Restraints and Structural Statistics[a]

total number of NOE distance restraints	836
intraresidue	316
sequential ($\|i - j\| = 1$)	206
medium ($\|i - j\| \leq 4$)	112
long ($\|i - j\| > 4$)	202
hydrogen bond constraints	20
dihedral angle restraints ϕ ($C_{(i-1)}$-N_i-$C_{\alpha i}$-C'_i)	19
distance constraint violations greater than 0.5 Å	0
dihedral angle constraint violations greater than 5°	0
r.m.s. deviations from experimental restraints	
distances (Å)	0.0064 ± 0.00243
dihedral angles (°)	0.472 ± 0.16406
r.m.s. deviation from idealized geometry	
bonds (Å)	0.003 ± 0.00022
angles (°)	0.608 ± 0.0228
impropers (°)	0.364 ± 0.0300
PROCHECK Ramachandran plot statistics	
residues in most favorable region	61.6%
residues in additionally allowed region	36.0%
residues in generously allowed region	1.7%
residues in disallowed region	0.7%
r.m.s. deviations of atomic coordinates	
total	
backbone (Å)	1.06
heavy atoms (Å)	1.08
secondary structures	
backbone (Å)	0.25
heavy atoms (Å)	0.97

[a] The total final energy is 120 kcal mol^{-1}. The nonbonded energy was calculated using a repel function with radii scaled by 0.8 of the standard values.

isomerization has been observed in the TFPI K2 domain (*9*) and bovine pancreatic trypsin inhibitor (*29*).

Approximate interproton distances were calculated from the cross-peak intensities on the ^{15}N edited 3D NOESY-HSQC and ^{13}C edited NOESY-HSQC spectra. The distance and angle restraints used for calculation are summarized in Table 1. None of the calculated structures had variations greater than 0.5 Å for the distance restraints and 5° for the dihedral angles. Figure 3a shows a stereoview of the backbone overlay of the 20 calculated structures. The root-mean-squares deviation (rmsd) value for the backbone atoms of these 20 structures was 1.06 Å for the overall molecule and 0.25 Å within the secondary structure elements. The ribbon representation of the average structure of the final ensemble of 20 structures is shown in Figure 3b. The quality of the obtained ensemble of structures was checked with the PROCHECK-NMR program (*28*), which showed that only 0.7% of the ϕ and ψ angles fell outside of the allowed regions of the Ramachandran plot. As seen in Figure 3, the structure of the TFPI K3 domain is the well-known Kunitz-type inhibitor fold that consists of two β-strands and one α-helix, and overall structure is very similar to the K2 domain (Figure 3c), with the rms deviation of 1.55 Å for the 58 defined C^α positions. Few NOEs are observed for residues Arg195 to Glu202 and Ser220 to Glu226, suggesting enhanced mobility of this region (Figure 3a).

Chemical Shift Changes of TFPI K3 Domain Upon Heparin Binding. Since it was reported that HBS-2 was located in the TFPI K3 domain between Gly 212 and Phe 243 (*15*), we investigated the changes of the ^1H-^{15}N NMR spectra of the TFPI K3 domain by adding an aliquot of heparin 16mer to identify the HBS-2 region. Upon addition of heparin, chemical shift changes were observed for some residues. The changes were almost saturated at the TFPI K3 domain/heparin molar ratio of 1:2. Figure 4a shows the chemical shift perturbation of H^N and N resonances for each residue between the free TFPI K3 domain and the heparin−TFPI K3 domain complex. The resonances of Gly185, Cys214, Leu236, Lys240, Lys241, and Gly242 showed significant chemical changes of >0.2 ppm upon heparin binding. Almost all of these residues are located around the α-helix (Figure 4b) except Gly185, suggesting that this region is HBS-2. In contrast, the chemical shifts of the other residues were not changed significantly, indicating that there were no large conformational changes affecting the overall structure of the molecule. We also performed the same experiment using heparin 4mer and 8mer and obtained the same results (data not shown). The reason Gly185 is affected by heparin binding is that it is located in an unstructured region (N-terminus) and it may be quite sensitive to any small changes.

Thus, we confirmed that HBS-2 lies around the α-helix region (Leu236, Lys240, Lys241, and Gly242), which forms a positive charge cluster in the TFPI K3 domain described below.

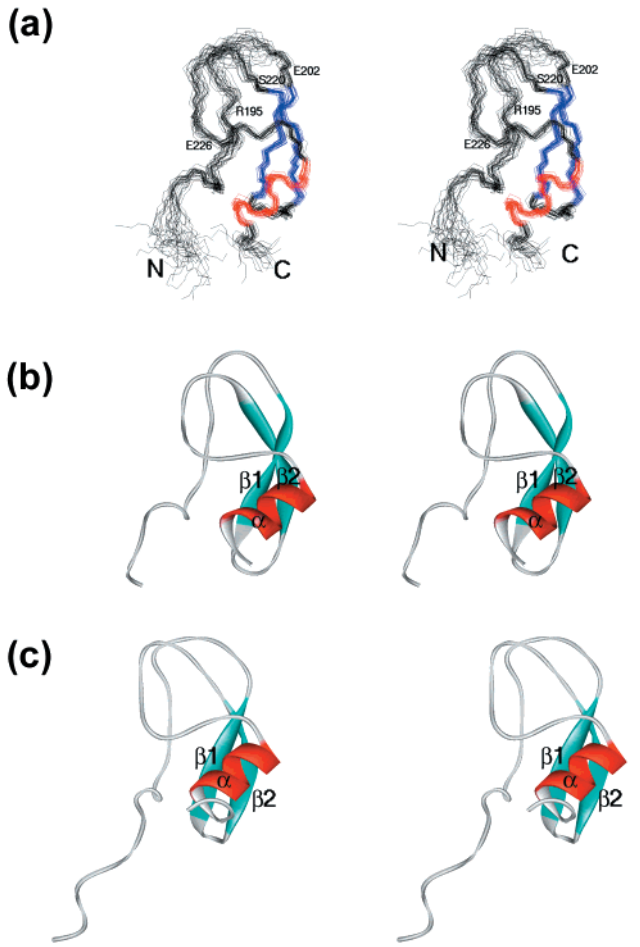

FIGURE 3: Three-dimensional structure of the TFPI K3 domain. (a) Overlay of backbone traces of 20 NMR solution structures. The α-helix and β-sheet are colored in red and blue, respectively. The poorly defined regions (R195−E202 and S220−E226) are also shown. (b) Ribbon representation of the mean structure of the TFPI K3 domain and (c) the K2 domain (1ADZ) in stereoview, generated using MOLMOL (*45*).

DISCUSSION

Surface Potential of TFPI K3 and K2 Domains. The heparin-binding sites of proteins usually contain clusters of

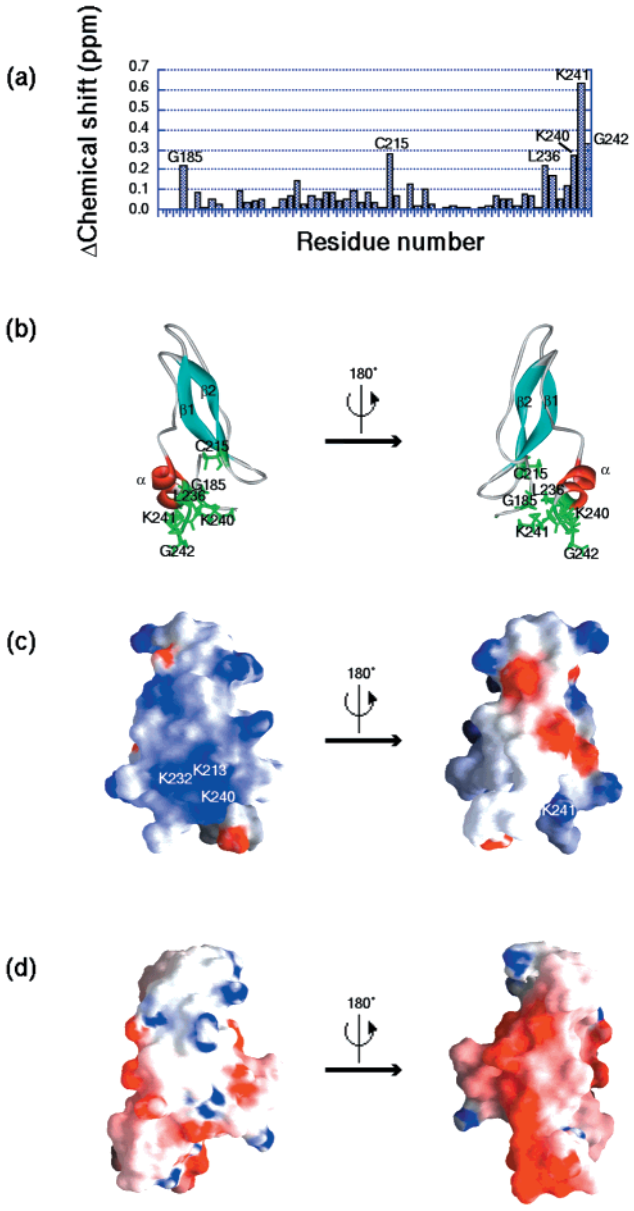

FIGURE 4: Binding of heparin 16mer to the TFPI K3 domain. (a) Chemical shift differences of each amino acid residue of the TFPI K3 domain between complexed and uncomplexed forms with heparin 16mer. (b) The location of the amino acid residues with a chemical shift perturbation of more than 0.2 ppm are shown in green. The two views are related by a rotation of 180° about the vertical axis. (c) Electrostatic surface representation of the TFPI K3 domain and (d) the K2 domain (1ADZ). Blue indicates regions of positive potential and red regions of negative potential. Surface view from the same orientation as in panel b. The figures were produced using the program GRASP (*46*).

basic amino acid residues, which provide positively charged regions for binding to the acidic groups of heparin (*30*). The positively charged clusters can be divided into two types, one featuring a cluster of consecutive basic amino acid residues and the other coordinating several basic residues in different positions by forming a specific conformation. In the case of TFPI, the C-terminal basic portion (HBS-1) is of the former type; however, the K3 domain (HBS-2) is of the latter because nine basic residues in the K3 domain (Arg199, Arg204, Lys213, Arg215, Lys218, Lys232, Arg237, Lys240, and Lys241) are not presented in consecutive positions.

A representation of the surface electrostatic properties of the TFPI K3 domain is shown in Figure 4c. The structure reveals that three basic residues (Lys213, Lys232, and Lys240) form a continuous patch of positive charge. The residues whose chemical shifts are perturbed significantly upon heparin binding are located in this positively charged cluster. This is the reason Cys214, Leu236, and Gly242, which are not basic residues, showed appreciable chemical shift changes on heparin binding. Reduction of the disulfide bonds of a synthetic peptide Gly212−Phe243 (a part of the K3 domain whose disulfide bond is formed by chemical reactions) results in a marked loss of function, suggesting that the native K3 domain structure is essential for the binding (*15*). Although the TFPI K2 domain has seven basic residues (Lys93, Arg107, Arg112, Lys120, Arg124, Lys126, and Lys144), it does not have heparin-binding activity. Unlike the K3 domain, the basic residues of the K2 domain do not form a cluster for fitting to the sulfate groups on heparin oligosaccharides (Figure 4d). There are also 10 acidic residues on this surface, which cancel positive charges totally. The three-dimensional structure of the K1 domain has not been determined yet, but it is reported that the K1 domain does not harbor a heparin-binding site (*15*). It also has no positively charged clusters even though 10 basic residues are in it.

In spite of the structural similarities between the TFPI K2 and K3 domain (Figure 3b,c), the K2 domain interacts with factor Xa and the K3 domain is apparently without inhibitory function (*31*). Petersen et al. (*8*) examined the different properties of the TFPI K2 domain and the K3 domain using putative three-dimensional models derived from a comparative molecular-modeling method. Computational docking into trypsin suggests that some features of the contact region of the TFPI K3 domain contribute to preventing close interaction of this domain with serine proteases. Their model indicates that Ser220 and the Cys198−Cys222 disulfide bond restrict the entry of the TFPI K3 domain into the substrate binding pocket of trypsin by steric hindrance. It is suggested that the lack of trypsin inhibitory activity of the TFPI K3 domain is the result of the opposite chirality of the Cys198−Cys222 disulfide bond as compared to that of Cys106−Cys130 in the K2 domain (*8*). However, as described above, our results show that the Cys198−Cys222 disulfide bond can adopt a variety of conformations, and an isomerization of this disulfide bond often takes place in solution. On the other hand, steric hindrance of the disulfide bond (Cys106−Cys130) also occurred in the putative TFPI K2 domain-factor Xa complex (*9*), suggesting that the opposite chirality of the Cys198−Cys222 disulfide bond is not the reason for the lack of inhibitory activity of the K3 domain. Thus, the surface electrostatic properties of TFPI appear to be important for the interaction with factor Xa. The putative complex structure of factor Xa-TFPI K2 domain revealed that three charged clusters of the K2 domain interacted with the active site cleft of factor Xa (*9*) (Figure 5). In this complex, Tyr109 facilitated the formation by the basic moiety of Lys126 of a positively charged cluster with Arg112 and Arg124, and this cluster would approach the acidic 39-loop of factor Xa. Further attractive electrostatic interactions could be afforded by Glu138 and Glu142 with LysF62 (residue of factor Xa is denoted with the prefix F) of factor Xa, and by an acidic patch (Glu100, Glu101, Asp102, and Glu124) with the basic

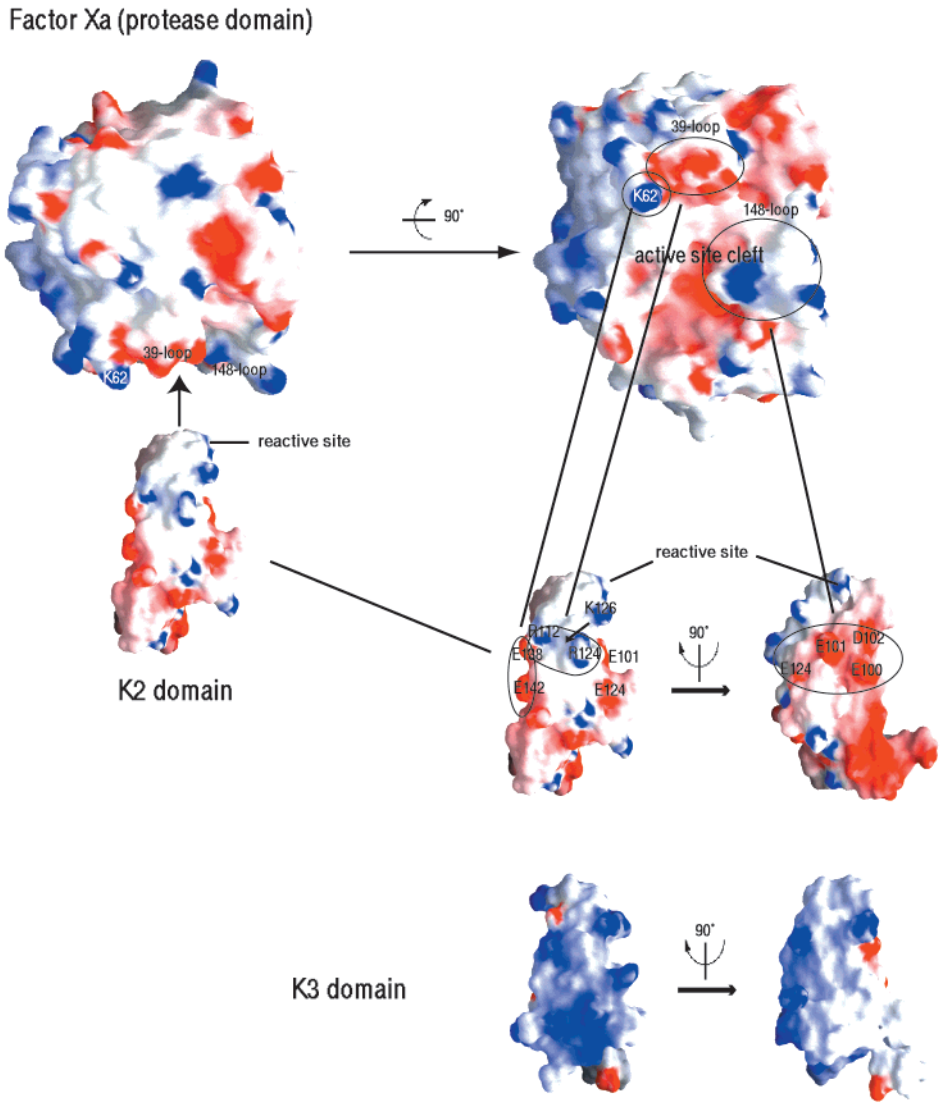

FIGURE 5: Surface representation of the electrostatic potential of the protease domain of factor Xa (1XKB), the TFPI K2 domain (1ADZ), and the K3 domain. Red and blue represent negative and positive potentials, respectively. The rotation of the protease domain of factor Xa is 90° about the horizontal axis, and the TFPI K2 and the K3 domains is 90° about the vertical axis. The surface orientation of the K2 and the K3 domains is the same. Residues involved in the binding interface between factor Xa and the TFPI K2 domain are labeled. The figures were produced using the program GRASP (*46*).

148-loop of factor Xa. By comparing these charged clusters of the K2 domain with those of the K3 domain, it is clear that the relative positioning of charged clusters is different in the K3 domain (Figure 5). Electrostatic interactions could serve to orient the inhibitor to the enzyme and provide the energy needed to reorganize residues in the active site cleft of factor Xa. Therefore, we suggested that the lack of inhibitory activity of the K3 domain arose from the absence of electrostatic interaction with factor Xa over a large surface area.

Implication for the Mechanism of Heparin Binding. In this study, we determined the solution structure of the TFPI K3 domain and identified the heparin binding site. It is of note that although TFPI contains three Kunitz-type domains, each domain has a different function. The results presented here and in previous reports (*9*, *10*) indicate that the function of each domain is closely related to their surface electrostatic potentials.

TFPI binds to lipoprotein, heparin, and proteoglycans on vascular endothelial cells, and the process is supposed to be mediated by the TFPI K3 domain and C-terminal basic region (*15*, *32*). Understanding the importance of the C-terminal portion of TFPI, we also prepared an NMR sample of the TFPI K3 domain that possesses the C-terminal end (K3C; Glu182−Met276) to determine its solution structure and to identify HBS-1. In the absence of heparin, the ^{1}H-^{15}N-HSQC spectrum showed that HN signals arose from the C-terminal portion of K3C clustered around 8.2 ppm (data not shown). This means that the C-terminal end is disordered and does not have a secondary structure. However, in the presence of heparin, K3C caused significant aggregation due to the high protein concentration for NMR. We are now trying to find out the most appropriate conditions for NMR measurements and hope to report the results soon.

The heparin-binding site of a serine protease inhibitor (serpin) is pivotal not only in regulating the inhibitory specificity of serpin but also in directing serpin to its target tissues to perform its function (*33*−*35*). The mechanisms of the heparin-accelerating protease inhibition have been explained as follows. First, binding of heparin induces con-

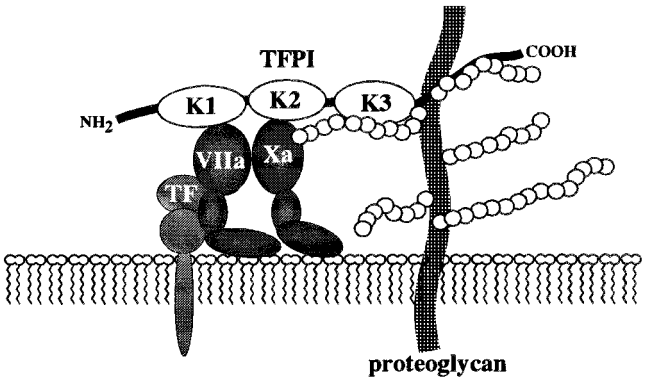

FIGURE 6: A diagram of the proposed model for the binding of heparin-bound TFPI to VIIa/TF and Xa on the surface of vascular endothelial cells. The TFPI K1 and K2 domains interact with VIIa/TF and Xa, respectively. The TFPI K3 domain and C-terminal portion bind to heparin (in the form of heparan sulfate proteoglycans on the cell surface).

formational changes favorable for the binding of serpins with protease (*35*−*38*). Second, heparin acts as a template to bind serpin and protease and thus enhance the association of both molecules (*39*, *40*). In the case of TFPI, the enhancement of inhibitory activity by heparin is probably not due to a conformational change of TFPI itself because the CD spectrum for TFPI or TFPI-ΔC did not change in the presence of heparin (Enjyoji et al., unpublished result). Our results also indicate that the K3 domain does not change its conformation upon heparin binding (Figure 4a).

TFPI is mainly localized on endothelial cells (*41*, *42*) and possibly associates with proteoglycans on the surface, and TFPI is released by the infusion of heparin. Although it is wondered whether TFPI-ΔC could also bind to proteoglycans on the cell surface, it is reported that TFPI isolated from the culture medium of transformed baby hamster kidney cells was essentially devoid of its C-terminal basic portion (*13*) and the cell bound TFPI-ΔC was released by heparin (*43*), suggesting that TFPI-ΔC can bind to proteoglycans. Furthermore, TFPI circulating in plasma is in the C-terminal truncated form (*44*). From these results, HBS-2 is important as is HBS-1, and we assume that heparin simply increases the local concentration of factor Xa and TFPI on the surface and stabilizes the initial complex formed on heparin (Figure 6).

Finally, we conclude that both HBS-1 and HBS-2 of TFPI play significant roles in the regulation of thrombosis in vivo, and our identification of a heparin-binding site in the TFPI K3 domain could provide significant insights into the structural and functional relationship of TFPI. Furthermore, our results also indicate that despite structural similarities between the TFPI K2 and K3 domains, each electronic surface potential has a different biological function, and the data pave the way for further studies of the regulation and the physiological function of TFPI.

ACKNOWLEDGMENT

S.M. thanks to Dr. Y. Goto (Osaka University) for helpful suggestions of the fermentation of *P. pastoris*.

REFERENCES

1. Davie, E. W., Fujikawa, K., and Kisiel. W. (1991) *Biochemistry 30*, 10363−10370.
2. Novotny, W. F., Girard, T. J., Miletich, J. P., and Broze, G. J., Jr. (1989) *J. Biol. Chem. 264*, 18832−18837.
3. Broze, G. J., Girard, T. J., and Novotny, W. F. (1990) *Biochemistry 29*, 7539−7546.
4. Sandset, P. M., Abildgaard, U., and Larsen, M. L. (1988) *Thromb. Res. 50*, 803−813.
5. Lindahl, A. K., Abildgaard, U., and Stokke, G. (1990) *Thromb. Res. 59*, 651−656.
6. Novotny, W. F., Palmier, M., Wun, T. C., Broze, G. J., and Miletich, J. P. (1991) *Blood 78*, 394−400.
7. Broze, G. J., Warren, L. A, Novotny, W. F., Higuchi, D. A., Girard, J. J., and Miletich, J. P. (1988) *Blood 71*, 335−343.
8. Petersen, L. C., Bjorn, S. E., Olsen, O. H., Nordfang, O., Norris, F., and Norris, K. (1996) *Eur. J. Biochem. 235*, 310−316.
9. Burgering, M. J., Orbons, L. P., van der Doelen, A, Mulders, J., Theunissen, H. J., Grootenhuis, P. D., Bode, W., Huber, R., and Stubbs, M. T. (1997) *J. Mol. Biol. 269*, 395−407.
10. Zhang, E., St. Charles, R., and Tulinsky, A. (1999) *J. Mol. Biol. 285*, 2089−2104.
11. Nordfang, O., Bjorn, S. E., Valentin, S., Nielsen, L. S., Wildgoose, P., Beck, T. C., and Hedner, U. (1991) *Biochemistry 30*, 10371−10376.
12. Lindahl, A. K., Abildgaard, U., and Staalesen, R. (1991) *Thromb. Res. 64*, 155−168.
13. Wun, T. C. (1992) *Blood 79*, 430−438.
14. Wesselschmidt, R., Likert, K., Huang, Z., MacPhail, L., and Broze, G. J. (1993) *Blood Coagulation Fibrinolysis 4*, 661−669.
15. Enjyoji, K., Miyata, T., Kamikubo, Y., and Kato, H. (1995) *Biochemistry 34*, 5725−5735.
16. Cifonelli, J. A. (1976) Nitrous acid depolymerization of glucosaminoglycans, in *Methods in Carbohydrate Chemistry* (Whistrler, B. L., and BeMiller, J. N., Eds.) Vol. VII, pp 139−142, New York, Academic Press.
17. Nagasawa, K., and Inoue, Y. (1980) De-*N*-sulfation, in *Methods in Carbohydrate Chemistry* (Whistler, B., BeMiller, J. N., Eds.) Vol. III, pp 291−294, New York: Academic Press.
18. Bitter, T., and Muir, H. M. (1962) *Anal. Biochem. 4*, 330−334.
19. Garrett, D. S., Powers, R., Gronenborn, A. M., and Clore, G. M. (1991) *J. Magn. Reson. 95*, 214−220.
20. Delaglio, F., Grzesiek, S., Vuister, G. W., Zhu, G., Pfeifer, J., and Bax, A. (1995) *J. Biomol. NMR. 6*, 277−293.
21. Bax, A., Clore, G. M., and Gronenborn, A. M. (1990) *J. Magn. Reson. 88*, 425−431.
22. Bax, A., and Ikura, M. (1991) *J. Biomol. NMR. 1*, 99−104.
23. Wittekind, M., and Mueller, M. (1993) *J. Magn. Reson. B, 101*, 201−205.
24. Muhandiram, D. R., Farrow, N. A., Xu, G.-Y., Smallcombe, S. H., and Kay, L. E. (1993) *J. Magn. Reson. B, 102*, 317−321.
25. Marion, D., Driscoll, P. C., Kay, L. E., Wingfield, P. T., Bax, A., Gronenborn, A. M., and Clore, G. M. (1989) *Biochemistry 28*, 6150−6156.
26. Kay, L. E., and Bax, A. (1990) *J. Magn. Reson. 86*, 110−126.
27. Brünger, A. T. (1992). *X-PLOR Version 3.1: A System for X-ray Crystallography and NMR*. Yale University Press, New Haven.
28. Laskowski, R. A., Rullmannn, J. A., MacArthur, M. W., Kaptein, R., and Thornton, J. M. (1996) *J. Biomol. NMR 8*, 477−486.
29. Otting, G., Leipinsh, E., and Wüthrich, K. (1993) *Biochemistry 32*, 3571−3582.
30. Cardin, A. D., and Weintraub, H. J. (1989) *Arteriosclerosis 9*, 21−32.
31. Girard, T. J., Warren, L. A., Novotny, W. F., Likert, K. M., Brown, S. G., Miletich, J. P., and Broze, G. J. (1989) *Nature 338*, 518−520.
32. Valentin, S., Nordfang, O., Bregengard, C., and Wildgoose, P. (1993) *Blood Coagulation Fibrinolysis 4*, 713−720.
33. Priglinger, U., Geiger, M., Bielek, E., Vanyek, E., and Binder, B. R. (1994) *J. Biol. Chem. 269*, 14705−14710.
34. Shirk, R. A., Elisen, M. G., Meijers, J. C., and Church, F. C. (1996) *Arterioscler., Thromb., Vasc. Biol. 16*, 1138−1146.

35. Jin, L., Abrahams, J. P., Skinner, R., Petitou, M., Pike, R. N., and Carrell, R. W. (1997) *Proc. Natl. Acad. Sci. U.S.A. 94*, 14683−14688.
36. Owen, B. A., and Owen, W. G. (1990) *Biochemistry 29*, 9412−9417.
37. Evans, D. L., Marshall, C. J., Christey, P. B., and Carrell, R. W. (1992) *Biochemistry 31*, 12629−12642.
38. Ersdal-Badju, E., Lu, A., Zuo, Y., Picard, V., and Bock, S. C. (1997) *J. Biol. Chem. 272*, 19393−19400.
39. Griffith, M. J. (1982) *J. Biol. Chem. 257*, 7360−7365.
40. Pratt, C. W., Whinna, H. C., and Church, F. C. (1992) *J. Biol. Chem. 267*, 8795−8801.
41. Bajaj, M. S., Kuppuswamy, M. N., Saito, H., Spitzer, S. G., and Bajaj, S. P. (1990) *Proc. Natl. Acad. Sci. U.S.A. 87*, 8869−8873.
42. Werling, R. W., Zacharski, L. R., Kisiel, W., Bajaj, S. P., Memoli, V. A., and Rousseau, S. M. (1993) *Thromb. Haemost. 69*, 366−369.
43. Callander, N. S., Rao, L. V., Nordfang, O., Sandset, P. M., Warn-Cramer, B., and Rapaport, S. I. (1992) *J. Biol. Chem. 267*, 876−882.
44. Broze, G. J., Lange, G. W., Duffin, K. L., and MacPhail, L. (1994) *Blood Coagulation Fibrinolysis 5*, 551−559.
45. Koradi, R., Billeter, M., and Wütrich, K. (1996) *J. Mol. Graph. 14*, 51−55.
46. Nicholls, A., Sharp, K. A., and Honig, B. (1991) *Proteins 11*, 281−296.

BI011299G